Efficient Low-Temperature Oxidation of Carbon-Cluster Anions by SO_2

Andrew J. Leavitt,*,†,‡ Richard B. Wyrwas,‡,§ William T. Wallace,‡,|| Daniel S. Serrano,† Melissa G. Arredondo,‡ Logan M. Leslie,† Farooq A. Khan,† and Robert L. Whetten*,‡

Department of Chemistry, University of West Georgia, Carrollton, Georgia 30118, and School of Chemistry and Biochemistry, Georgia Institute of Technology, Atlanta, Georgia 30332-0400

Received: January 6, 2005; In Final Form: May 11, 2005

Carbon-cluster anions, C_N^-, are very reactive toward SO_2 (sticking probability of 0.012 ± 0.005 for C_{27}^- at 25 °C), in contrast to their inertness toward other common atmospheric gases and pollutants. In flow reactor experiments at ambient temperature and near atmospheric pressure, primary adsorption of SO_2 by the carbon cluster anions, $N = 4-60$, yields $C_NSO_2^-$ or $C_{N-1}S^-$. The inferred elimination of neutral CO_2 is also detected as meta-stable decay in collision-induced dissociation. At higher temperatures, the reaction of SO_2 with nascent carbon clusters yields $C_{N-1}SO^-$ as well as undetected CO. The size-dependent initial reactivity reflects the previously established structural transitions (i.e., from chain to cyclic to cage structures). Such carbon clusters are formed in sooting flames and may act as nuclei for the formation of primary soot particles and serve as models for the local structural features of active soot particle sites for black-carbon soot. The facile generation of reactive carbon-sulfide and -sulfinate units may therefore have implications for understanding the health and environmental effects attributed to the coincidence of soot and SO_2.

Introduction

Concentrated atmospheric emissions of black-carbon (soot) particulates and SO_2 coincide in many parts of the world as a result of incomplete combustion of fossil fuel and biomass. An estimated 12−24 Tg of carbon soot is emitted annually into the troposphere from biomass combustion and anthropogenic sources such as diesel engines and coal-fired power plants.[1,2] The simultaneous presence of these agents has been linked to death from lung cancer and heart disease.[3] However, the nature of any such cooperative interaction between SO_2 and soot particulates remains unclear, despite long study.[4] Among the possible mechanisms of soot−SO_2 interaction, soot may efficiently adsorb SO_2, thereby concentrating it in the lungs where subsequent processes lead to damage. Soot could also catalyze the oxidation of SO_2 to SO_3 (H_2SO_4) as first suggested in 1974 by Novakov et al[5] and by others more recently[6−8] (a homogeneous gas-phase or aqueous reaction involving photogenerated OH radicals is the accepted dominant reaction pathway for global-scale production of atmospheric H_2SO_4[9,10]). Finally, soot could react stoichiometrically with SO_2, modifying either the soot particle or SO_x into more harmful species. Carbon−SO_2 interactions are also relevant in environmental remediation since activated carbon is used to remove SO_2 from hot flue gases.[11−13]

It has been shown that carbon clusters are generated in sooting flames and act as the precursors to the larger (∼5 nm) primary soot particles.[14,15] Carbon soot particles as small as 10 nm in diameter have been detected in sooting flames using differential mobility analysis.[16] Primary soot particles are defect-rich multishell structures with active sites for adsorption, involving unpaired electrons, or negative charging. Carbon cluster anions can thus serve as well-defined models for defect sites in soot. Carbon-cluster anions, C_N^-, have been extensively studied.[17−19] They are generally highly stable (high electron affinity) species with established chain, -ring, and -cage structures, sharing these characteristics with active soot.[18,19] By contrast, carbon cluster cations (C_N^+) and neutrals are more reactive toward a variety of atmospheric gases such as O_2, N_2O, and SO_2.[20−23]

The complete oxidation of carbon−graphite by SO_2 is favorable (−23 kcal mol^{-1}), but it is immeasurably slow except at elevated temperatures. Humeres et al.[11] recently studied the reduction of SO_2 on activated carbon at elevated temperatures. Using reactor partial pressures of 0.20 atm of SO_2 at a temperature of 600 °C, the dominant products were CO_2 and S_2. Above 630 °C, CO and COS were formed in significant amounts. Here, we address these questions by investigating the size-selective reactions of carbon-cluster anions with SO_2 vapor in an atmospheric-pressure fast-flow reactor at ambient temperature.

Experimental Procedures

The reaction of SO_2 with C_N^- occurred in a near atmospheric pressure, variable-temperature fast-flow reactor, and the products were detected by time-of-flight mass spectrometry, following standard procedures.[24] Figure 1 shows the schematic features of the cluster source flow reactor.[25,26] The cooled clusters enter the flow reactor and mix with a flow of a dilute 1.5% SO_2/He gas mixture for up to 0.10 ms as the clusters traversed the length of the flow reactor (15 or 25 mm). In the absence of fast, in situ thermometry, we have been very concerned to establish that these SO_2 reactions are taking place with properly thermalized carbon-cluster anions. Toward this end, we have carried out a long series of control reactions, with various reactants introduced in the same manner and over the same concentration range as for SO_2. In each cycle of operation, the source gas-

* To whom correspondences should be addressed. Phone: (770) 836-4550; e-mail: alaevitt@westga.edu.
† University of West Georgia.
‡ Georgia Institute of Technology.
§ Current address: Department of Chemistry, Indiana University, Bloomington, IN 47405-7102.
|| Current address: Department of Chemistry, Texas A&M University, College Station, TX 77842-30012.

10.1021/jp050087g CCC: $30.25
Published on Web 06/22/2005

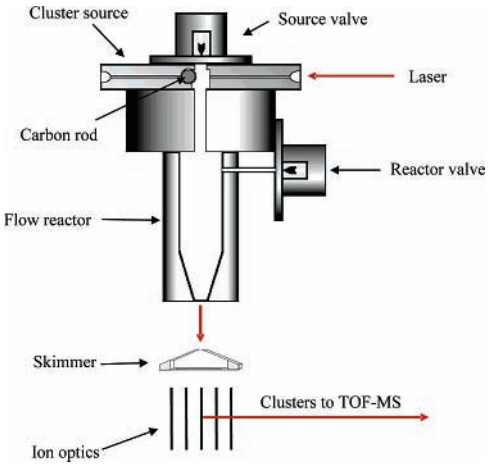

Figure 1. Schematic of the pulsed cluster source with atmospheric pressure flow reactor. Carbon clusters of various sizes and charge states are produced by laser ablation (Nd:YAG, 355 nm) of a graphite rod, entrained, and thermalized in the primary He flowstream. The exit orifice of the flow reactor is tapered down from the reaction channel diameter of 6 mm to a diameter of 3 mm to ensure turbulent mixing of the reactants.

valve opens and delivers pulses (0.3 ms long, 20 mm^3 displaced volume) of high-pressure (8 atm) helium gas. The peak pressure in the flow reactor can thus approach 0.5 bar because of the choked exit-flow and modest (15-fold) volume expansion. Carbon clusters of various sizes and charge states are produced by laser ablation (Nd:YAG, 355 nm) of a graphite rod, entrained, and thermalized in the primary He flowstream. This packet merges with the reactant flowstream—a longer, weaker flow of SO_2 in He carrier—introduced from a second gas-valve, which opens at a variable delay with respect to the cluster-packet arrival. The SO_2 concentration in the reactor exceeds that of all the carbon clusters combined. The SO_2 partial pressure in the reactor is estimated to be approximately 0.08% of the total pressure (approaching 0.4 mbar), as calculated from the prepared dilution (1.5% for reactor insertion) in He and the instantaneous relative intensities (1:20) of the two gas pulses, as measured on a fast ionization gauge. The exit orifice of the flow reactor is tapered down from the reaction channel diameter of 6 mm to a diameter of 3 mm to ensure turbulent mixing of the reactants. The transit time of the clusters through the reactor is estimated at 90 μs, corresponding to a 300 m/s flow speed (Mach-0.2 for He at this temperature). During this period, a carbon-cluster is estimated to undergo thermalizing collisions with helium atoms on the order of 10^5 to 10^6, depending on cluster size, and on the order of 10^2 encounters with SO_2. Such values are normally sufficient to establish the high-pressure limit of bimolecular reaction kinetics, as well as to ensure thermodynamic control in the case of reversible adsorption processes. After leaving the flow reactor, the jet containing reactants and products expands into vacuum, is skimmed, and enters the pulsed-voltage extraction region of the time-of-flight mass spectrometer equipped with a reflectron.

Results and Discussion

The C_N^- clusters react with SO_2 to form stable products under ambient temperature and near-atmospheric conditions at ~230 ppm of SO_2 at a total flow reactor pressure estimated at 0.3 bar. Figure 2 shows the mid- and low-*N* mass regions of the resultant mass spectra with and without the addition of SO_2 to the flowstream of thermalized (wall temperature ~300 K) C_N^- clusters. In Figure 2A, a reference spectrum (lower) is produced

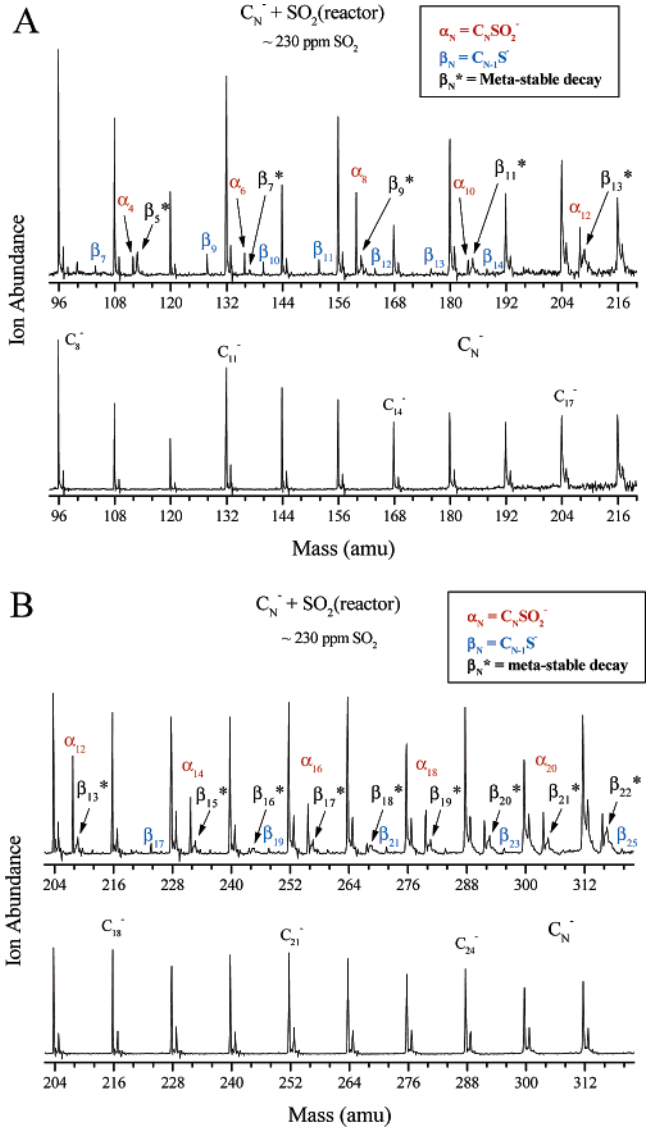

Figure 2. (A) Mid-*N* mass spectra of thermalized carbon cluster anions, C_N^-, in the region of C_{17}^- to C_{26}^- without (below) and with (above) exposure to a 1.5% SO_2/He stream in the flow reactor at room temperature (P_{SO2} = 0.14 mbar). The addition of SO_2 leads to the appearance of new peaks in the mass spectrum corresponding to ambient-temperature reactions producing $C_NSO_2^-$ (α_N) and $C_{N-1}S^-$ (β_N). (B) Same conditions as panel A but for low-*N* mass in the region of C_8^- to C_{18}^-. Increasing the partial pressure of SO_2 in the reactor drives the reaction toward completion.

SCHEME 1

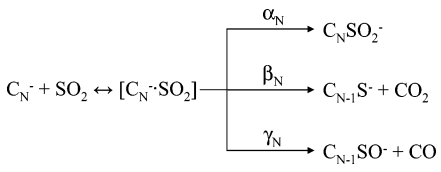

when the reactor gas flow is offset temporally from the source gas flow to show unreacted C_N^- clusters only for $N = 17-26$. In Figure 2A (upper), the flows are overlapping, and both product and reactant peaks are present. In a separate experiment, the low-*N* mass region ($N = 8-18$) with and without the addition of SO_2 under the same conditions is shown in Figure 2B.

Scheme 1 shows the primary reactions proposed to account for product identities found in the mass analysis. The efficient reaction of thermalized carbon anion clusters, C_N^-, with a dilute

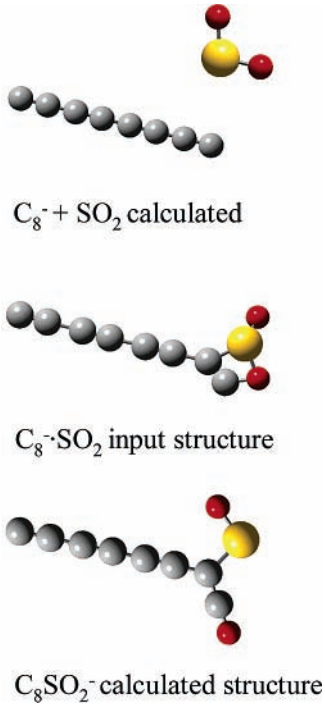

Figure 3. Calculated structures of C_8^-, SO_2, and $C_8SO_2^-$. The optimized structures of the stable product $C_8SO_2^-$ (below) were left unconstrained. The starting geometry for the intermediate state of $C_8SO_2^-$ (middle), terminal sulfinate,[11] is shown and was assembled using molecular mechanics.

mixture of SO_2 in helium at ambient temperature yields $C_NSO_2^-$ (α_N), C_NS^- (β_N), and C_NSO^-(γ_N), accompanied by the (undetected) evolution of CO_2 and CO across a cluster size range of $N = 4-80$. The presence of the CO_2 product was confirmed indirectly as a meta-stable decay neutral. Under the same experimental conditions, no adsorption or reaction products due to the interaction of O_2, NO, or the much more strongly oxidizing N_2O with C_N^- were detected. The interaction of NO_2 with certain C_N^- does produce barely detectable amounts of associated products.

Using carbon-cluster anions (C_N^-) as a surrogate for carbon soot, comparisons of the heats of formation of C_N^- and C_N and their reaction products containing -SO_2 were made for the smaller clusters $N = 8$ and 9, where accurate theoretical treatment is available. Many structural models were considered—and actually calculated[27−30]—for the initial and intermediate products of SO_2−cluster interactions in an attempt to identify plausible reaction mechanisms. Energies for optimized ground-state configurations (linearly constrained) of carbon chains were calculated with density functional theory utilizing the hybrid exchange-correlational functional B3LYP at the 6-311+G** level. The optimized structures of the stable product $C_8SO_2^-$ was left unconstrained. The starting geometry for the intermediate state of $C_8SO_2^-$, terminal sulfinate,[11] is shown and was assembled using molecular mechanics. All quantum chemical calculations were conducted with the *Gaussian 03* computational package. Attempts to optimize certain cyclic addition structures, suggested by known organic analogues as well as XPS results on activated carbon,[11] led to the identification of strongly bound intermediates, depicted in Figure 3 and Table 1. The table contains the heats of reaction for the linear carbon clusters, C_N^m reacting with SO_2 to produce $C_NSO_2^m$.

These calculations suggested that the reactions listed in Table 1 are favorable with the exception of the $C_9SO_2^-$ species that is slightly endothermic. Figure 3 shows the calculated structures

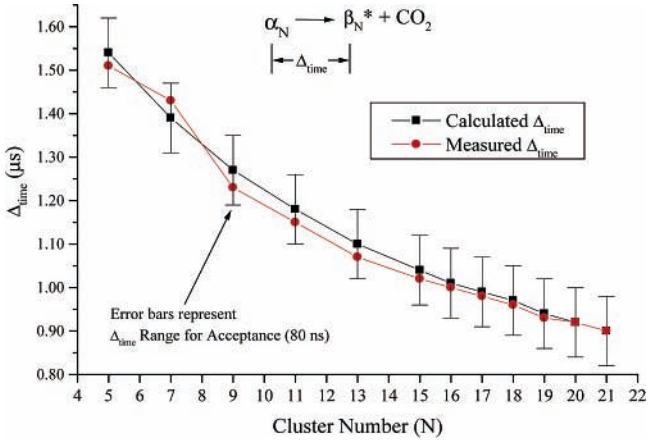

Figure 4. Calculated vs the measured time difference between the arrival at the detector of a stable product ion and a daughter ion as the result of a meta-stable decay. An α_N product can dissociate (decay) while in the field-free region of the TOF mass spectrometer. By assuming the loss of CO_2, a calculation can reveal when the fragmented ion will be detected. This assumption is verified when the measured Δ_{time} is within 80 ns of the calculated value, a time range represented by the vertical error bars. All meta-stable products appearing in Figure 3 can be assigned α_N products decaying to β_N* and CO_2.

TABLE 1

C_N	$C_N^m + SO_2 \rightarrow C_NSO_2^m$ $\Delta H_{reaction}$ (kcal mol^{-1})	
N	neutral $m = 0$	anion $m = -1$
8	−28	−60
9	−19	+0.4

for C_8^- and $C_8SO_2^-$ using density functional theory.[27−30] The α_N and β_N products contain one sulfur each as confirmed by an isotopic-abundance analysis of the product peak groupings (*m*, *m + 1*, *m + 2*) in higher SO_2 concentration spectra revealing the presence of both C (^{13}C, *m + 1*) and S (^{34}S, *m + 2*). As the SO_2 concentration is increased in the flow reactor, the abundance of products increase relative to that of unreacted C_N^- clusters, suggesting that the reaction can be driven toward completion.

The reaction mass spectra (Figure 3) also show the presence of broad peaks located near to the α_N product peaks. These broad peaks, β_N*, were assigned to the delayed loss of CO_2 and appear every ~24 amu ($N = 5-15$) and then every 12 amu ($N = 16$ and higher). These peaks were assigned to the meta-stable decay of weakly adsorbed species during the flight in the field-free region of the TOF spectrometer.[31] These meta-stable peaks were calculated to be the result of the loss of weakly bound CO_2. Figure 4 shows the comparison of the calculated time difference and the measured time difference between the stable product and its charged daughter fragment that would occur during the field free flight if the product lost CO_2. This process is represented by

$$C_NSO_2\ (\alpha_N) \rightarrow C_{N-1}S^-\ (\beta_N^*) + CO_2 \qquad (1)$$

The meta-stable peaks occur at 24-u spacings in the low-mass region (89, 113, 137, 161, 185, 209, and 233 u) and then shift to a 12-u spacing in the higher mass region (245, 257, 269, ..., 665 u). Each one of these meta-stable peaks can be assigned to the meta-stable decay of the low mass α_{odd-N} cluster from $N = 5-15$ and then α_N (even and odd) from $N = 16$ and higher to produce the corresponding β_N cluster and CO_2.

Preliminary results obtained by heating or cooling the reactor indicate that the α_N process decreases with increasing temperature, suggesting that it is a nonactivated, reversible binding,

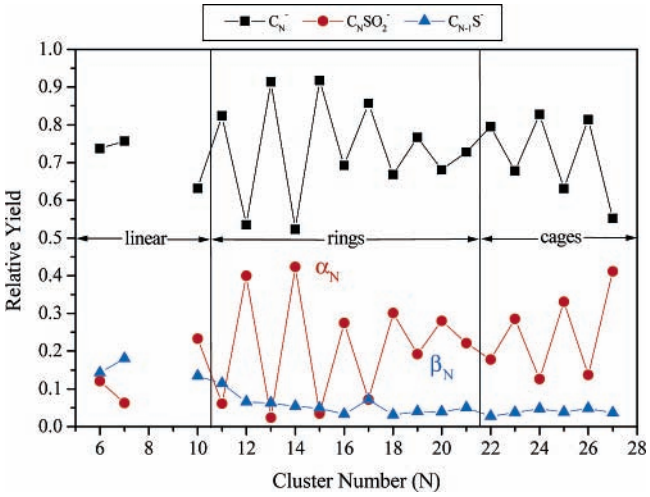

Figure 5. Relative reaction yield for each carbon cluster anion is shown with regions of defined reactivity. Previous structural assignments of linear, rings, and polycycles or cages were correlated with reactivity. Although linear structures dominate from $N = 4-10$, only $N = 6$ and 7 are shown. Generally, even-N clusters are more reactive in this linear region. Ring structures dominate from $N = 11-21$ showing the greatest extent of reaction for all isomers with a very strong odd−even dependence favoring the even-N clusters. The cage structures dominate from $N = 22$ and higher as evidenced by a strong odd−even N dependence on the extent of reaction. This dependence could be attributed to the simple adsorption of one or more SO_2 molecules to the less reactive even-N cluster (fullerene structure) as compared to the more reactive odd cluster (nonfullerene structure).

whereas the β_N process increases with temperature, consistent with an activated, irreversible process (CO_2 elimination), as also concluded from the analysis of the metastable decay process (collisional activation leading to dissociation).

Figure 5 shows the extent of reaction versus cluster size, for the reaction channels in Scheme 1. These were calculated from the abundances from Figure 2 where no attempt was made to account for the meta-stable (β_N*) decay products. An odd−even N reaction dependence is observed throughout the cluster sizes studied. Even-N C_N^- clusters are more reactive (fewer parent C_N^- clusters remain) from $N = 6-20$ while odd-N C_N^- clusters are more reactive from $N = 21-27$.

This size dependence can be explained by the well-established transitions in the structural and electronic characteristics of the C_N^- anions. Previously, Gotts et al. measured size-dependent isomers for both the positive and the negative ions of carbon.[32] For the carbon cluster anion, linear isomers dominate up to $N = 9$, ring structures dominate from $N = 10-40$, and fullerenes are possible from $N = 35$ and greater, although cluster source conditions can affect the distribution of isomers. Given the higher pressures used in this study, fullerenes may be present in greater abundance and at lower cluster sizes than depicted in the work of Gotts et al. From $N = 23$ and higher, this odd−even effect could be due to the presence of caged carbon structures where even-numbered clusters produce fullerenes (less reactive). Note that all carbon cluster anions are open-shell radicals in which no preferential odd−even N effect is seen in the pure C_N^- mass spectrum.[32] The lack of an electronic effect points to structural considerations in developing an explanation of the relative intensities.

To explore higher temperature reaction channels, SO_2 was seeded into the source buffer gas to allow for the simultaneous presence of SO_2 and nascent carbon clusters at the moment just after the laser ablation of carbon. The carbon clusters are present with a higher partial pressure of SO_2, free electrons, and higher

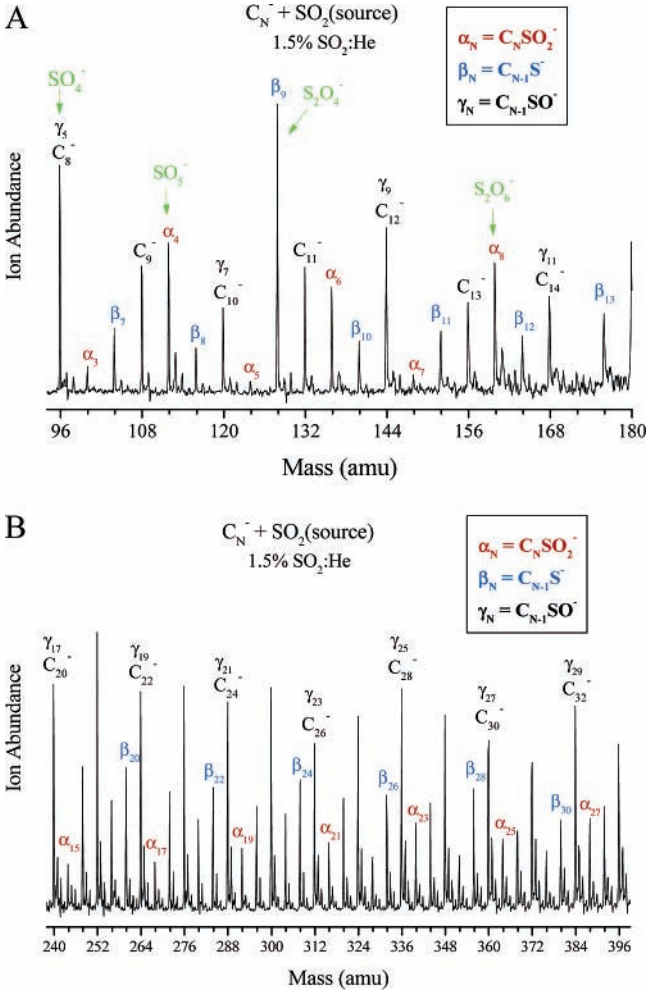

Figure 6. (A) Low-N mass spectra of thermalized carbon cluster anions, C_N^-, in the region of C_8^- to C_{15}^- without (A) and with (B) exposure to a dilute amount of 1.5% SO_2/He in the cluster source at room temperature. In addition to $C_NSO_2^-$ (α_N) and $C_{N-1}S^-$ (β_N), the product $C_{N-1}SO^-$ (γ_N) was identified. (B) Same as panel A but showing region C_{20}^- to C_{33}^-. The formation of $C_NSO_2^-$ (α_N) for odd-N clusters is not favored from $N = 11-21$. By $N = 23$, the formation of $C_NSO_2^-$ (α_N) for odd-N clusters is slightly favored over even-N clusters.

reaction temperatures than present in the reactor. Figure 6A shows the resultant low-N mass spectrum from the injection of SO_2 in the cluster source. As in the case of the reactor experiments described previously, the α_N ($C_NSO_2^-$) and β_N (C_NS^-) products are present. On close inspection of the unreacted C_N^- peaks, an isotopic abundance analysis reveals a significantly enhanced ($m + 2$) peak confirming the presence of ^{34}S. Thus, sulfur is present in a reaction product that is mass coincident with C_N^-. A product assignment based upon the third reaction in Scheme 1 was assumed.

$$C_N^- + SO_2 \leftrightarrow [C_N^- \cdot SO_2] \rightarrow C_{N-1}SO^- (\gamma_N) + CO \quad (2)$$

Given that no meta-stable decay peaks are apparent in the spectrum, a straightforward conversion of C_N^- to the α_N, β_N, and γ_N products is inferred. Preliminary results obtained by heating or cooling the reactor indicate that the α_N process decreases with increasing temperature, suggesting that it is a nonactivated, reversible binding, whereas the β_N process increases with temperature, consistent with an activated, irreversible process (CO_2 elimination), as also concluded from the analysis of the meta-stable decay process (collisional activation leading to dissociation). In the low-N spectrum, the

even-N clusters ($N = 8$ and 10) do not undergo partial oxidation to produce CO. Finally, SO_2 introduced in the flow reactor can produce cluster anions ($S_nO_m^-$) where $n = 1$ and 2 and $m = 2-6$, due to their favorable electron affinities.[33,34] These ($S_nO_m^-$) peaks are mass coincident with both parent and product peaks thus adding to the apparent intensity (area) of the peak.

Figure 6B shows the high-N mass spectrum of C_N^- reacting with SO_2 seeded in the source gas. Since the γ_N product peak is mass coincident with the C_N^- parent peak, quantitative analysis of the extent of reaction is not possible under these conditions. The odd-N α_N products ($N = 11-17$) are not favored when compared to their corresponding β_N products and perhaps γ_N products. This suggests that the α_N product is most likely unstable (higher energy), preferring conversion to the β_N and γ_N products. As N increases, the even-N clusters become less reactive, while the reactivity of the odd-N clusters increases. By C_{23}^-, no odd−even alternation is discernible, possibly due to the addition of the γ_N product to the remaining C_N^- peak masking any intensity alternation.

As compared to other black-carbon soot models, such as graphite, activated carbons, or lab-generated soot, the carbon clusters show extraordinarily higher activity for adsorption and reaction with SO_2. The sticking probability was estimated to be 0.012 ± 0.005 for C_{27}^- at 45% depletion at ambient temperature under the experimental conditions used. For example, under conditions where the SO_2 partial pressure is estimated (from previous calibrated experiments) at 0.015 Torr, the C_{27}^- cluster is found to be depleted by 45% as a result of 20 encounters. To estimate the number of encounters, one multiplies the geometrical cross-section for these species, 0.9 nm^2; their rms speeds, 340 m/s; the SO_2 concentration; and the transit time, 90 μs. This estimate is quite different from the uptake coefficient (0.002) of SO_2 on n-hexane soot at −100 °C reported by Koehler et al.[8] and underscores the importance of the reactive site in n-hexane. n-Hexane will contain a vastly lower density of reactive sites when compared to the carbon cluster anions. This likely reflects the greater concentration of exposed reactive sites and the unrestricted access to such points. Additionally, when compared to other atmospheric gases such as O_2, NO, N_2O, and H_2O, the SO_2 molecule has over twice the electron affinity (1.107 eV) than the next gas. Couple this with the observation that multiple adsorption of SO_2 on even the largest clusters appears not to be occurring, a strong interaction between SO_2 (high electron affinity) and the anionic sites of the clusters could possibly explain this reactive behavior.

Conclusion

As compared to other black-carbon soot models, such as graphite, activated carbons, or lab-generated soot, the carbon clusters show extraordinary higher activity for adsorption and reaction with SO_2. The unexpected ambient-temperature oxidation of the carbon cluster anions by SO_2 to produce $C_NSO_2^-$, $C_{N-1}S^-$, $C_{N-1}SO^-$, CO, and CO_2 that has been observed may suggest an alternate mechanism for the uptake of SO_2 in the troposphere where C_N^- serves as a surrogate for carbon soot. The size-dependent initial reactivity reflects the previously established cluster structural transitions (i.e., from linear-chain to cyclic to cage structures). The possible production of carbon−sulfur compounds in point source plumes that goes on to participate in other atmospheric reactions and play a role in the soot−SO_2 health issues raises questions for further study. This study provides an example of the use of clusters to model the interaction of small particles such as soot with environmentally relevant gases in the atmosphere.

Acknowledgment. The authors thank Drs. C. Foote, P. Wine, D. Sherrill, D. DeSilva, and R. Weber for stimulating discussions. Additionally, J. Bradshaw and D. Doby were helpful in the initial stages of this work. This work has been supported by the National Science Foundation of the United States and the RSEC (Research Sites for Educators in Chemistry) program (A.J.L.).

References and Notes

(1) Chughtai, A. R.; Atteya, M. M. O.; Kim, J.; Konowalchuk, B. K.; Smith, D. W. *Carbon* **1998**, *36*, 1573.
(2) Grassian, V. H. *J. Phys. Chem. A* **2002**, *106*, 860.
(3) Pope, C. A., III; Burnett, R. T.; Thun, M. J.; Calle, E. E.; Krewski, D.; Ito, K.; Thurston, G. D. *J. Am. Med. Assoc.* **2002**, *287*, 1132.
(4) Posfai, M.; Anderson, J. R.; Buseck, P. R.; Sievering, H. *J. Geophys. Res.* **1999** *104*, 21, 685.
(5) Novakov, T.; Chang, S. G.; Harker, A. B. *Science* **1974**, *186*, 259.
(6) Schumann, U.; Strom, J.; Busen, R.; Baumann, R.; Gierens, K.; Krautstrunk, M.; Schroder, F. P.; Stingl, J. *J. Geophys. Res.* **1996**, *101*, 6853.
(7) Fahey, D. W.; Keim, E. R.; Boering, K. A.; Brock, C. A.; Wilson, J. C.; Jonsson, H. H.; Anthony, S.; Hanisco, T. F.; Wennberg, P. O.; Miake-Lye, R. C.; Salawitch, R. J.; Louisnard, N.; Woodbridge, E. L.; Gao, R. S.; Donnelly, S. G.; Wamsley, R. C.; Del Negro, L. A.; Solomon, S.; Daube, B. C.; Wofsy, S. C.; Webster, C. R.; May, R. D.; Kelly, K. K.; Loewenstein, M.; Podolske, J. R.; Chan, K. R. *Science* **1995**, *270*, 70.
(8) Koehler, B. G.; Nicholson, V. T.; Roe, H. G.; Whitney, E. S. *J. Geophys. Res.* **1999**, *104*, 5507.
(9) Hynes, A. J.; Wine, P. H. In *Gas-Phase Combustion Chemistry*; Gardiner, W. C., Jr., Ed.; Springer-Verlag: New York, 2000; p 343.
(10) Finlayson-Pitts, B. J.; Pitts, J. N., Jr. *Chemistry of the Upper and Lower Atmosphere*; Academic Press: San Diego, 2000; p 9.
(11) Humeres, E.; Peruch, M. B.; Moreira, R. F. P. M.; Schreiner, W. *J. Phys. Org. Chem.* **2003**, *16*, 824.
(12) Wiltowski, T. S.; Sangster, K.; O'Brien, W. S. *J. Chem. Technol. Biotechnol.* **1996**, *67*, 204.
(13) Panagiotidis, T.; Richter, E.; Juntgen, H. *Carbon* **1988**, *26*, 89.
(14) Gerhardt, P.; Löffler, S.; Homann, K. H. *Chem. Phys. Lett.* **1987**, *137*, 306.
(15) Reilly, P. T. A.; Gieray, R. A.; Whitten, W. B.; Ramsey, J. M. *J. Am. Chem. Soc.* **2000**, *122*, 11596.
(16) Higgins, K. J.; Jung, H.; Kittelson, D. B.; Roberts, J. T.; Zachariah, M. R. *J. Phys. Chem. A* **2002**, *106*, 96.
(17) Dugourd, P.; Hudgins, P. R.; Tenenbaum, J. M.; Jarrold, M. F. *Phys. Rev. Lett.* **1998**, *80*, 4197.
(18) Maier, J. P. *J. Phys. Chem. A* **1998**, *102*, 3462.
(19) Kohno, M.; Suzuki, S.; Shiromaru, H.; Moriwaki, T.; Achiba, Y. *Chem. Phys. Lett.* **1998**, *282*, 330.
(20) Zhang, Q. L.; O'Brien, S. C.; Heath, J. R.; Liu, Y.; Curl, R. F.; Kroto, H. W.; Smalley, R. E. *J. Phys. Chem.* **1986**, *90*, 525.
(21) McElvany, S. W.; Dunlap, B. I.; O'Keefe, A. *J. Chem. Phys.* **1987**, *86*, 715.
(22) Zimmerman, J. A.; Eyler, J. R.; Bach, S. B. H.; McElvany, S. W. *J. Chem. Phys.* **1991**, *94*, 3556.
(23) Fisher, K.; Hopwood, F.; Dance, I.; Willett, G. *New J. Chem.* **1999**, *23*, 609.
(24) Knickelbein, M. B. *Annu. Rev. Phys. Chem.* **1999**, *50*, 79.
(25) Salisbury, B. E.; Wallace, W. T.; Whetten, R. L. *Chem. Phys.* **2000**, *262*, 131.
(26) Wallace, W. T.; Whetten, R. L. *J. Phys. Chem. B* **2000**, *104*, 10964.
(27) Giuffreda, M. G.; Deleuze, M. S.; Francois, J. P. *J. Phys. Chem. A* **2002**, *106*, 8569.
(28) Wang, H. Y.; Huang, R. B.; Chen H.; Lin, M. H.; Zheng, L. S. *J. Phys. Chem. A* **2001**, *105*, 4653.
(29) Lee, C.; Yang, W.; Parr, R. G. *Phys. Rev. B* **1988**, *37*, 785.
(30) Becke, A. D. *J. Chem. Phys.* **1993**, *98*, 5648.
(31) Wallace, W. T.; Whetten, R. L. *Eur. Phys. J. D* **2001**, *16*, 123.
(32) Gotts, N. G.; von Helden, G.; Bowers, M. T. *Int. J. Mass Spectrom. Ion Processes* **1995**, *149/150*, 217.
(33) Mohler, O.; Reiner, T.; Arnold, F. *J. Chem. Phys.* **1992**, *97*, 8233.
(34) Wang, X. B.; Nicholas, J. B.; Wang, L. S. *J. Phys. Chem. A* **2000**, *104*, 504.